New Evidence for Spatio-temporal Fragmentation in the Solar Flare Energy Release

R. Ramesh[1], V. Mugundhan[2], and K. Prabhu[1]
[1] Indian Institute of Astrophysics, Koramangala 2nd Block, Bangalore, Karnataka, 560034, India
[2] Raman Research Institute, Sadashiva Nagar, Bangalore, Karnataka, 560080, India
Received 2019 November 7; revised 2020 January 9; accepted 2020 January 9; published 2020 January 24

Abstract

We analyzed a group of type III radio bursts and a Hα flare from the Sun that were observed simultaneously on 2015 January 14. The radio observations were in the spectral mode over the frequency range 85–35 MHz, and separately in the imaging mode at 80 MHz. The duration of the observations was $\approx$6 minutes. The centroids of the type III bursts and the Hα flare were independently scattered near the associated active region. But the displacements in the centroids of the two phenomenon are correlated with each other. This indicates that the individual bursts in a group of type III radio bursts are most likely due to flaring activity at different locations in the active region at different times during the same flare interval.

Unified Astronomy Thesaurus concepts: Solar activity (1475); Solar coronal radio emission (1993); Solar flares (1496); Solar chromosphere (1479); Radio bursts (1339); Solar x-ray flares (1816); Solar corona (1483); Solar magnetic fields (1503); Solar magnetic reconnection (1504)

1. Introduction

Type III radio bursts from the Sun are signatures of energetic ($\sim$1–100 keV) electrons propagating upward through the corona into the interplanetary medium along open magnetic field lines. They are due to electron acceleration at the magnetic reconnection sites in the corona above the associated active region (Cairns et al. 2018). The emission mechanism of the bursts is widely believed to be due to plasma processes. Due to the coherent nature of the latter, the bursts are easily observable and hence they are a unique tool to understand the aforementioned electron acceleration. The bursts are observed typically in the frequency range $\approx$1 GHz–10 kHz. Since the electron density (N_e) and hence plasma frequency (f_p) decreases outward in the solar atmosphere, the above frequency range corresponds to heliocentric distances from the low corona to beyond the orbit of Earth. This implies that type III bursts are the tracers of magnetic connectivity between the solar surface, the corona, and the interplanetary medium. In radiospectrograph records, the type III bursts can be observed to drift from high to low frequencies at speeds $\sim$0.1c–0.3 c (see, e.g., Wild et al. 1963; Wild & Smerd 1972; Dulk 1985; Bastian et al. 1998; Reid & Ratcliffe 2014).

Type III bursts commonly occur in groups. It has been pointed out that the individual bursts in a group are due to acceleration episodes occurring at different locations in the same active region (Benz 1994; Vlahos & Raoult 1995). Observations showing displacements in the centroid of the type III burst during the course of the event are there in the literature (Kane et al. 1980; Raoult & Pick 1980; Trottet et al. 1982; Lantos et al. 1984; Raoult et al. 1985; Gopalswamy & Kundu 1987; Pick & Ji 1987; Ramesh et al. 2003, 2005; Morosan et al. 2014; Bisoi et al. 2018). But reports on the correspondence between such changes (particularly for the type III bursts in a group where the possibilities of observing the positional shifts are more likely due to the comparatively longer duration of the event) and locations of the maximum emission in the associated Hα flare (assumed to be the sites of the electron acceleration) are rare. Considering that spatially resolved observations[3] are difficult at present, in the present work we had attempted to verify the aforementioned association by inspecting the inter-pixel changes in the respective images (Mas et al. 2016).

2. Observations

The radio observations were carried out using the different facilities operated by the Indian Institute of Astrophysics (IIA) in the Gauribidanur Observatory[4] (Ramesh 2011; Ramesh et al. 2014). The radio spectral images were obtained with the Gauribidanur LOw-frequency Solar Spectrograph (GLOSS) in the frequency range 85–35 MHz (Ebenezer et al. 2001, 2007; Kishore et al. 2014; Hariharan et al. 2016). The GLOSS has a one-dimensional array of eight log-periodic dipole (LPD) antennas along a north–south baseline. The half-power width of the response pattern of GLOSS is $\approx$90° $\times$ 6° (R.A. $\times$ decl.) at the highest frequency of operation, i.e., 85 MHz. While the width of the response pattern along R.A. is nearly independent of frequency, its width along the decl. varies inversely with the frequency due to interferometric arrangement of the individual antennas. The observations were in the swept-frequency mode over the aforementioned frequency range with a sweep time $\approx$250 ms. The number of data points acquired in each sweep is 400. The observing bandwidth and dwell time at each frequency are $\approx$125 kHz and $\approx$625 ns, respectively. The antenna and the receiver systems were calibrated by carrying out observations in the direction of the Galactic center as described in Kishore et al. (2015). The two-dimensional radio images were obtained with the Gauribidanur RAdioheliograPH (GRAPH) at 80 MHz (Ramesh et al. 1998, 1999a, 2006). The GRAPH is a T-shaped radio interferometer array of LPDs and it has an angular resolution of $\approx$4′ $\times$ 6′ (R.A. $\times$ decl.) at the above frequency. The

---

[3] Two independent point sources are regarded as just resolved when the principal diffraction maximum of one image coincides with the first minimum of the other.
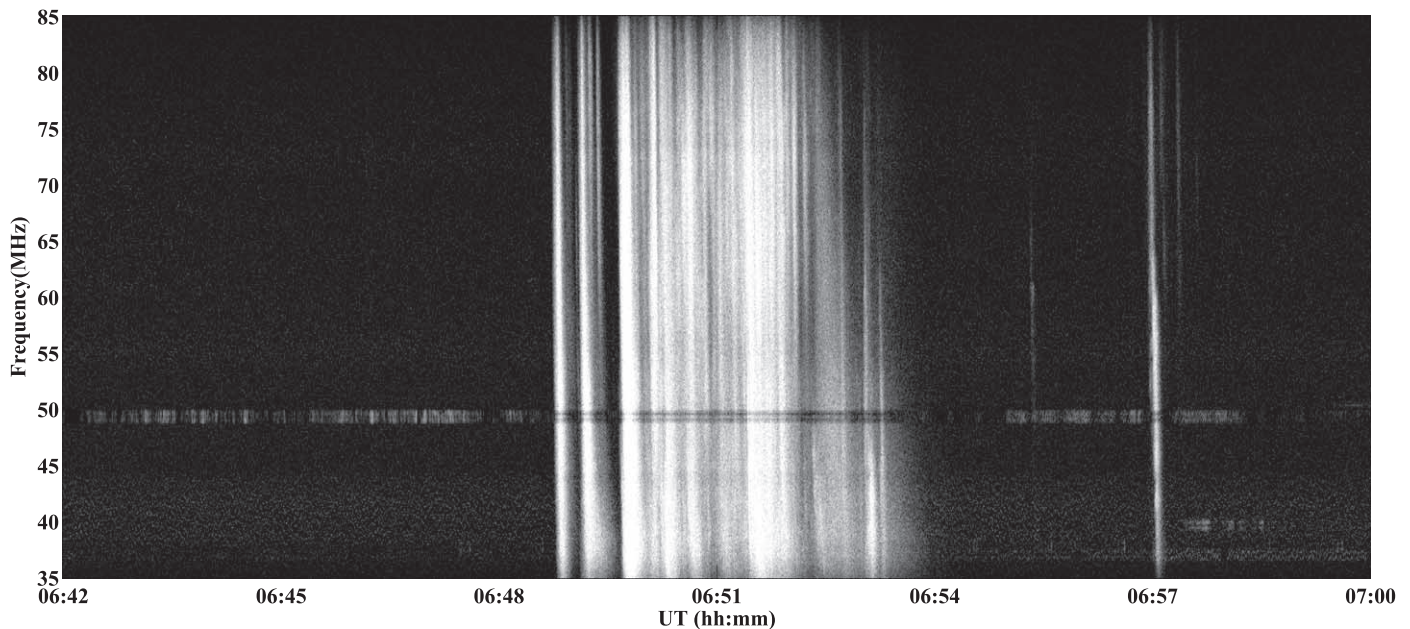
[4] https://www.iiap.res.in/?q=centers/radio

Figure 1. Dynamic spectrum of the solar radio emission observed with GLOSS on 2015 January 14 in the time interval ≈06:42–07:00 UT. The intense patch of fast drifting emission from high to low frequencies during ≈06:48–06:54 UT corresponds to a group of type III solar radio bursts. The individual bright emission near ≈06:57 UT is an isolated type III burst. The horizontal patch near 50 MHz is due to local radio frequency interference.

integration time is ≈250 ms and the observing bandwidth is ≈2 MHz. The field of view (FOV) in the GRAPH images is ≈2° × 2°, and the pixel size is ≈14″. The GRAPH data were calibrated using the standard Astronomical Image Processing System. We also used data obtained with the Gauribidanur Radio Interferometer Polarimeter (GRIP; Ramesh et al. 2008), Gauribidanur RAdio Spectro-Polarimeter (Sasikumar Raja et al. 2013a; Hariharan et al. 2015; Kishore et al. 2015; Mugundhan et al. 2018b), and e-CALLISTO (Monstein et al. 2007; Benz et al. 2009). The combined use of the aforementioned imaging, spectral, and polarimetric data help to understand the radio signatures associated with the corresponding solar activity in a better manner (see, e.g., Sasikumar Raja & Ramesh 2013b). The optical data were obtained with the Hα telescope in the Kodaikanal Solar Observatory (KSO) of IIA with a time cadence of ≈1 minute. The FOV in the Hα images is ≈41′ × 41′, and the pixel size is ≈1″.2 (Ravindra et al. 2016).

Figure 1 shows the GLOSS observations on 2015 January 14 in the time interval 06:42–07:00 UT. The intense patch of emission during ≈06:48–06:54 UT corresponds to a group of type III bursts. The other separate similar bright and faint fast drifting features, but not as a group like the former, close to ≈06:55:30 UT and ≈06:57 UT are isolated type III bursts. There was an SF-class Hα flare on the same day from the active region AR 12259 located at the heliographic coordinates S14W02. The flare was observed during the period ≈06:49–07:04 UT with maximum at ≈06:52 UT. There was also a C2.3-class GOES soft X-ray flare in the time span ≈06:46–06:57 UT. Its maximum was at ≈06:51 UT.[5] A comparison of the different timings mentioned above indicates that the isolated type III bursts as well as the group of type III bursts occurred within the flare period. Figure 2 shows the GRAPH imaging observations of the type III burst at 80 MHz around ≈06:50:42 UT, overlaid on the KSO Hα image

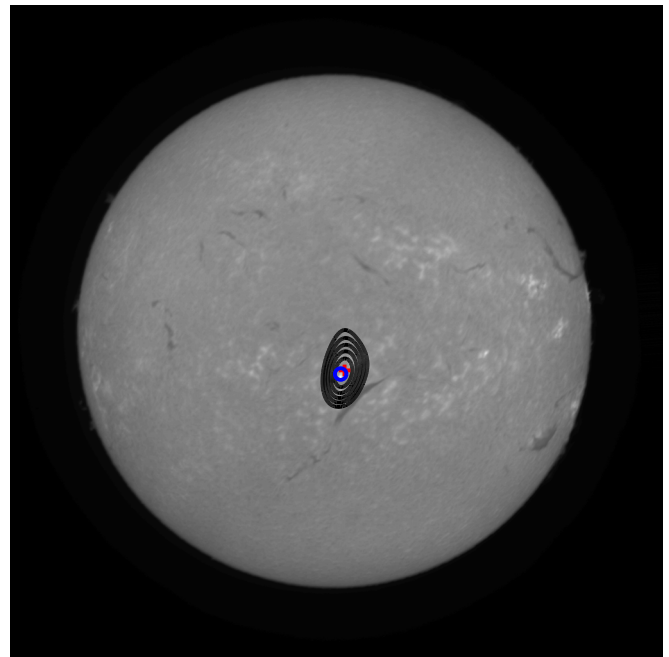**Figure 2.** GRAPH observations of the type III burst at ≈06:50:42 UT on 2015 January 14 superposed on the KSO Hα image obtained at the same time. The radio contours are shown until the 1/e level. The red "+" symbol is the centroid of the radio contours. The blue "o" symbol represents the centroid of the Hα flare. The uncertainties in the radio centroid position are ≈0″03 in the R.A. and decl. axes, respectively. The corresponding values for the Hα centroid are ≈0″01 along either axis.

obtained at the same time. There is an excellent spatial correlation between the locations of the burst and the aforementioned flare. Figure 3 shows the KSO Hα telescope observations of the flare light curve and Stokes I and V time profiles of the type III burst group observed with the GRIP at 80 MHz (over a bandwidth of ≈1 MHz) during the same time interval as in Figure 1, i.e., 06:48–06:54 UT. But for the fine
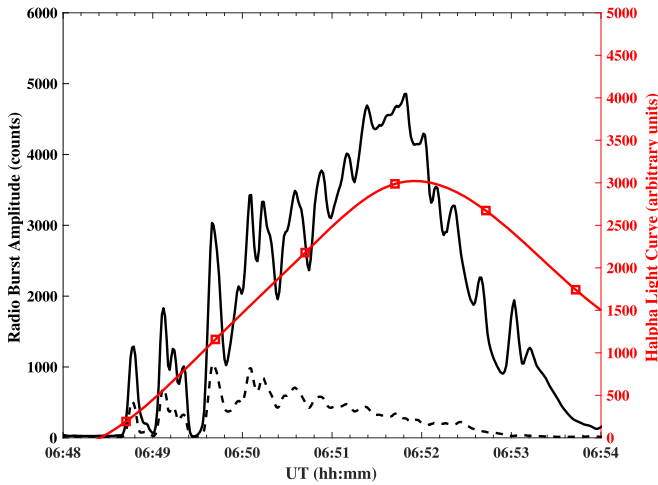

Figure 3. GRIP observations (at 80 MHz) of the Stokes I and V time profiles of the type III burst group in Figure 1, and the scaled light curve of the flare observed with the KSO Hα telescope during the same time interval. Shape preserving spline interpolation was used for the Hα light curve. The profiles (black color) in solid and dotted lines correspond to Stokes I and V emission, respectively.

structures in the radio bursts, there is a close similarity between the envelope of the bursts and the Hα light curve. The maximum amplitude of the type III burst group is at the same time as the flare maximum. This close association between the group of type III bursts observed with GLOSS as well as GRIP and the Hα light curve clearly indicates that the bursts are very much likely due to the said flaring activity. The spatial correspondence between the type III burst and Hα flare in Figure 2 also indicates the same. Note that the Hα data were obtained with a time cadence of $\approx$1 minute as compared to the GRIP data, which were obtained with an integration time of $\approx$250 ms. This could be the reason for the absence of the fine structures in the Hα light curve in the present case. The different peaks in the Stokes I profile correspond well with the individual bursts in Figure 1. The estimated degree of circular polarization (dcp) from the GRIP observations in the range $\approx$25%–50% during the early part of the burst ($\approx$06:49–06:51 UT). It decreases to $\lesssim$10% around flare maximum ($\approx$06:52 UT) and beyond.

Figure 4 shows the centroids of the type III bursts observed with the GRAPH at 80 MHz and the flare observed with the KSO Hα telescope, during the same period as the GLOSS observations in Figure 1. The centroid positions and the associated uncertainties were derived as follows: we selected $\approx$50 $\times$ 50 pixel wide regions of interest (RoIs) about the locations of the burst and the flare at any chosen time during the interval $\approx$06:48–06:54 UT. Then we used the following formulae to calculate the centroid ($\bar{x}$ and $\bar{y}$) in the x- and y-directions, independently for the burst and the flare, at the aforesaid chosen time: i.e., $\bar{x} = \frac{\sum x_i I(x_i)}{\sum I(x)}$ and $\bar{y} = \frac{\sum y_i I(y_i)}{\sum I(y)}$, where "$i$" is the pixel number, "$I$" is the intensity, and the summation is over all the pixels within the RoI. The error in the estimate is the standard deviation of each pixel with respect to the centroid, scaled by the total intensity (see Equations (44)–(47) in Kontar et al. 2019). In the case of radio observations, we found that the maximum (minimum) errors along the R.A. and decl. axes (x- and y-direction) are $\approx 0''\!.3$ ($\approx 0''\!.02$) and $\approx 0''\!.2$ ($\approx 0''\!.01$), respectively. The corresponding maximum (minimum) errors in Hα observations are $\approx 0''\!.04$ ($\approx 0''\!.01$) along the
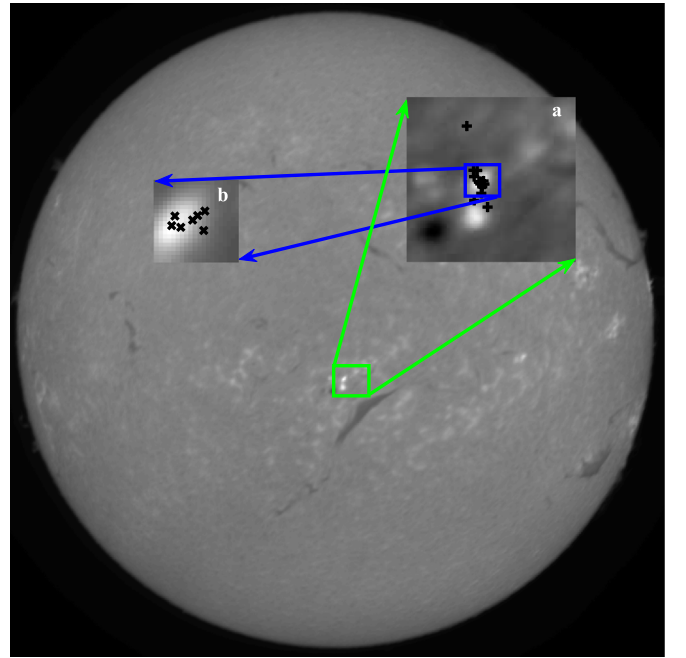

Figure 4. Composite picture showing the centroids of the type III bursts observed with the GRAPH at 80 MHz and the associated flare observed with the KSO Hα telescope, both overlaid on the KSO full disk Hα image obtained at $\approx$06:52:43 UT. The radio and flare centroids were obtained from the corresponding observations during the same interval as in Figure 1, i.e., $\approx$06:48–06:54 UT. Solar north is straight up and east is to the left. The two bright spots inside the "green" box correspond to the flaring activity in AR 12259 mentioned in Section 2. Inset "a" shows its zoomed view and the locations of the type III burst centroids ("+" symbol). Inset "b" shows the locations of the flare centroids ("x" symbol) w.r.t. the same brightenings.

x-direction, and $\approx 0''\!.02$ ($\approx 0''\!.01$) along the y-direction. The error was smaller when the source intensity was higher. Note that similar identification of centroid positions to an accuracy better than the angular resolution of the observing instrument was also recently reported by Kontar et al. (2017). The peak brightness temperature (T_b) of the type III bursts, estimated using the beam size of the GRAPH at 80 MHz, is $\sim 10^7$ K. This is certainly an underestimate by at least of two orders of magnitude since the "true" sources sizes of the type III bursts are expected to be $\lesssim 15''$ (Mugundhan et al. 2016, 2018a; Kontar et al. 2017). We would like to add here that ionospheric refraction effects on the radio source positions in the present case are expected to be very minimal since the observations were carried out close to the local noon during which time the zenith angle of the Sun is the least. Any positional shifts in hour angle and decl. due to ionospheric effects are expected to be negligible during that time. Note that the elevation of Sun on 2015 January 14 when the present observations were carried out was $\approx 60°$. Second, the total duration of the observations in the present case is only $\approx$6 minutes. This is less than the period ($\approx$20 minutes) over which radio source positions at low frequencies usually change due to ionospheric effects (Stewart & McLean 1982; Mercier 1996).

3. Analysis and Results

An inspection of Figure 4 shows that the Hα flaring activity is not confined to a single location. The centroid of emission is at different positions at different times during the flare period. Interestingly, the centroids of the type III bursts also exhibit a similar behavior. Each centroid in this case corresponds to the
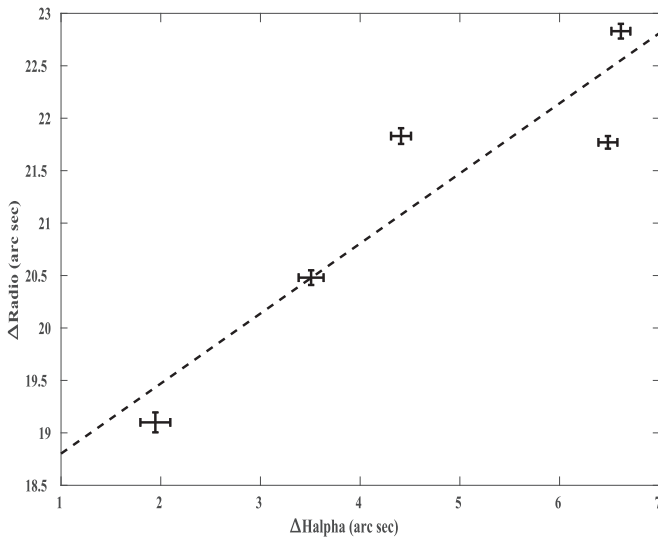
Figure 5. Angular separations of the type III burst and Hα flare centroids (see Figure 3) from AR 12259 (located at S14W02). The dashed line is the least-squares linear fit to the data points. The fit equation is $y = 0.668x + 18.13$, where y is ΔRadio, and x is ΔHalpha. The correlation coefficient is ≈0.9. Note that the dimensions of the "+" symbol representing each data point indicate the 5σ errors in the radio burst and flare centroid positions, at different instances of time during the interval ≈06:48–06:54 UT.

individual burst(s) in the group of type III bursts in Figures 1 and 3. The contemporaneous changes in both the Hα and radio centroids strongly suggests that the respective positional shifts are most likely related. Based on spectral observations of decimetric spikes, Benz (1985) had earlier concluded that the associated energy release is discontinuous and occurs at many different sites of size ≈200 km each. In the case of type III bursts, long baseline observations at 53 MHz had revealed that the angular size of the burst is ≲15″ (Mugundhan et al. 2018a). Occultation observations during solar eclipses and other studies have also indicated the presence of radio emitting structures on similar angular scales in the corona at low frequencies (Ramesh et al. 1999b, 2012; Ramesh & Sastry 2000; Ramesh & Ebenezer 2001; Kathiravan et al. 2011). The angular separations between majority of the Hα as well as radio centroids in Figure 4 are larger than the pixel sizes in the images obtained with the KSO Hα telescope (≈1″2) and GRAPH (≈14″), respectively (see Section 2). The angular sizes of the flare energy release sites and the type III radio bursts mentioned above are comparatively smaller. This indicates that each of the Hα and radio centroids in Figure 4 are independent.

To verify whether the changes in the positions of the Hα and radio centroids are correlated, we calculated their angular separations from AR 12259 (located at heliographic coordinates S14W02) at different times during the interval ≈06:48–06:54 UT using their respective running difference images. Only those Hα and radio images obtained at the same time in the above interval were used for the calculations. The results are shown in Figure 5. The errors associated with each data point are different from the rest since they varied with the intensity of flare and burst emission as mentioned earlier. The estimated separations are clearly larger than the pixel sizes in the respective images. Further, there is a striking correlation (≈90%) between the angular separations in the two cases. This clearly indicates that the individual bursts in the type III burst group (see Figures 1 and 3) are due to spatial and temporal fragmentation of the primary energy release near the flare site

in the chromosphere as revealed by the Hα observations. The observations of group of type III bursts are the coronal signatures of such a fragmented energy release. The temporal variation in the dcp of the type III bursts (see Figure 3 and Section 2) also possibly indicates radio emission originating from different locations above the active region. Note that dcp is related to the strength of the magnetic field and the latter is inhomogeneous at a given plasma level from where the radio emission at a particular frequency originates (Mercier 1990).

4. Summary

We have reported the first observational evidence for a correlation between the changes in the centroid positions of a group of type III radio bursts and that of the associated Hα flare emission. Similar optical and radio observations with high spatial resolution would be useful to understand the topic of fragmented energy release better since it has been addressed mostly using time and spectral domain studies to date (Aschwanden & Benz 1994; Benz 1994; Isliker & Benz 1994; Isliker 1996; Aschwanden 1999). The magnetic coupling between the different levels in the solar atmosphere and how the energetic particles are guided through the corona into the interplanetary space could also be probed using such observations (see, e.g., Klein et al. 2008).

References

Aschwanden, M. 1999, in The 9th European Meeting on Solar Physics, Magnetic Fields and Solar Processes, ed. A. Wilson (Paris: ESA), 1015
Aschwanden, M., & Benz, A. O. 1994, SSRv, 68, 193
Bastian, T. S., Benz, A. O., & Gary, D. E. 1998, ARA&A, 36, 131
Benz, A. O. 1985, SoPh, 96, 357
Benz, A. O. 1994, SSRv, 68, 135
Benz, A. O., Monstein, C., Meyer, H., et al. 2009, EM&P, 104, 277
Bisoi, S. K., Sawant, H. S., Janardhan, P., et al. 2018, ApJ, 862, 65
Cairns, I. H., Lobzin, V. V., Donea, A., et al. 2018, NatSR, 8, 1676
Dulk, G. A. 1985, ARA&A, 23, 169
Ebenezer, E., Ramesh, R., Subramanian, K. R., Sundara Rajan, M. S., & Sastry, C. V. 2001, A&A, 367, 1112
Ebenezer, E., Subramanian, K. R., Ramesh, R., Sundara Rajan, M. S., & Kathiravan, C. 2007, BASI, 35, 111
Gopalswamy, N., & Kundu, M. R. 1987, SoPh, 111, 347
Hariharan, K., Ramesh, R., & Kathiravan, C. 2015, SoPh, 290, 2479
Hariharan, K., Ramesh, R., Kathiravan, C., Abhilash, H. N., & Rajalingam, M. 2016, ApJS, 222, 21
Isliker, H. 1996, A&A, 310, 672
Isliker, H., & Benz, A. O. 1994, SSRv, 68, 185
Kane, S. R., Raoult, A., & Pick, M. 1980, ApJL, 241, L113
Kathiravan, C., Ramesh, R., Barve, I. V., & Rajalingam, M. 2011, ApJ, 730, 91
Kishore, P., Kathiravan, C., Ramesh, R., Rajalingam, M., & Barve, I. V. 2014, SoPh, 289, 3995
Kishore, P., Ramesh, R., Kathiravan, C., & Rajalingam, M. 2015, SoPh, 290, 2409
Klein, K.-L., Krucker, S., Lointier, G., & Kerdraon, A. 2008, A&A, 486, 589
Kontar, E. P., Chen, X., Chrysaphi, N., et al. 2019, ApJ, 884, 122
Kontar, E. P., Yu, S., Kuznetsov, A. A., et al. 2017, NatCo, 8, 1515
Lantos, P., Pick, M., & Kundu, M. R. 1984, ApJL, 283, L71
Mas, D., Perez, J., Ferrer, B., & Espinosa, J. 2016, ApOpt, 55, 4974
Mercier, C. 1990, SoPh, 130, 119
Mercier, C. 1996, AnGeo, 14, 42

Monstein, C., Ramesh, R., & Kathiravan, C. 2007, BASI, 35, 473
Morosan, D. E., Gallagher, P. T., Zucca, P., et al. 2014, A&A, 516, A67
Mugundhan, V., Ramesh, R., Barve, I. V., et al. 2016, ApJ, 831, 154
Mugundhan, V., Ramesh, R., Kathiravan, C., et al. 2018a, ApJL, 855, L8
Mugundhan, V., Ramesh, R., Kathiravan, C., Gireesh, G. V. S., & Hegde, A. 2018b, SoPh, 293, 41
Pick, M., & Ji, S. C. 1987, SoPh, 107, 159
Ramesh, R. 2011, in ASI Conf. Ser. 2, 1st Asia-Pacific Sol. Phys. Meeting, ed. A. R. Choudhuri & D. Banerjee (Pune: ASI), 55
Ramesh, R., & Ebenezer, E. 2001, ApJL, 558, L141
Ramesh, R., Kathiravan, C., Barve, I. V., & Rajalingam, M. 2012, ApJ, 744, 165
Ramesh, R., Kathiravan, C., Satya Narayanan, A., & Ebenezer, E. 2003, A&A, 400, 753
Ramesh, R., Kathiravan, C., Sundara Rajan, M. S., Barve, I. V., & Sastry, C. V. 2008, SoPh, 253, 319
Ramesh, R., Kathiravan, C., Sundara Rajan, M. S., Indrajit Barve, V., & Rajalingam, M. 2014, in ASI Conf. Ser. 13, Proc. of the Metrewavelength Sky, ed. J. N. Chengalur & Y. Gupta (Pune: ASI), 19
Ramesh, R., & Sastry, C. V. 2000, A&A, 358, 749
Ramesh, R., Satya Narayanan, A., Kathiravan, C., Sastry, C. V., & Udaya Shankar, N. 2005, A&A, 431, 353
Ramesh, R., Subramanian, K. R., & Sastry, C. V. 1999a, A&AS, 139, 179
Ramesh, R., Subramanian, K. R., & Sastry, C. V. 1999b, SoPh, 185, 77
Ramesh, R., Subramanian, K. R., Sundara Rajan, M. S., & Sastry, C. V. 1998, SoPh, 181, 439
Ramesh, R., Sundara Rajan, M. S., & Sastry, C. V. 2006, ExA, 21, 31
Raoult, A., & Pick, M. 1980, A&A, 87, 63
Raoult, A., Pick, M., Dennis, B. R., & Kane, S. R. 1985, ApJ, 299, 1027
Ravindra, B., Prabhu, K., Rangarajan, K. E., et al. 2016, RAA, 16, 127
Reid, H. A. S., & Ratcliffe, H. 2014, RAA, 14, 773
Sasikumar Raja, K., Kathiravan, C., Ramesh, R., Rajalingam, M., & Barve, I. V. 2013a, ApJS, 207, 2
Sasikumar Raja, K., & Ramesh, R. 2013b, ApJ, 775, 38
Stewart, R. T., & McLean, D. J. 1982, PASA, 4, 386
Trottet, G., Pick, M., House, L., et al. 1982, A&A, 111, 306
Vlahos, L., & Raoult, A. 1995, A&A, 296, 844
Wild, J. P., & Smerd, S. F. 1972, ARA&A, 10, 159
Wild, J. P., Smerd, S. F., & Weiss, A. A. 1963, ARA&A, 1, 291